International Journal of Computer Information Systems and Industrial Management Applications
ISSN 2150-7988 Volume 18(2) 2026 pp. 1913-1931
https://doi.org/10.70917/ijcisim-2026-5110
Article

Flow Direction Algorithm with Lévy Distribution and Random Opposition for Simultaneous Network Reconfiguration with DGs and SCs Integration

K. Kalyan Kumar[1], Dr. G. Nageswara Reddy[2]

[1]Research Scholar (Part-time), YSR Engineering College of Yogi Vemana University, Proddatur, & Assistant Professor, KSRMCE (A), Kadapa, Andhra Pradesh, India.
[2]Professor, Department of Electrical & Electronics Engineering, YSR Engineering College of Yogi Vemana University, Proddatur, Andhra Pradesh, India
Corresponding author mail id: kalyankumark13@gmail.com

Abstract: This article proposes an enhanced Flow Direction Algorithm (FDA) that integrates Lévy distribution and Random Opposition-Based Learning (ROBL) strategies to improve overall performance. First, the Lévy distribution is used to update the flow velocity vector, enabling a more accurate representation of movement toward the neighbour with the smallest objective function value, while introducing greater flexibility and randomness into velocity prediction. Second, ROBL refines the decision-making process during flow direction identification, enhancing the algorithm's adaptability. This promotes more effective exploration of potential solutions and strengthens convergence toward the optimal flow direction. The proposed ROFDA is comprehensively validated on simultaneous Optimal Network Reconfiguration (ONR) problems involving the integration of Distributed Generators (DGs) and Shunt Capacitors (SCs). Results clearly demonstrate that jointly optimizing network reconfiguration with DGs and SCs integration achieves significantly greater power loss minimization than optimizing each approach individually. Evaluated on standard 33-bus and 69-bus test systems, ROFDA consistently outperforms existing variants, including FDA, OFDA, and MFDA, thereby confirming its effectiveness, robustness, and superiority as an advanced optimization framework for solving complex power distribution network problems.
Keywords: Flow Direction Algorithm, Lévy Distribution, Random Opposition-Based Learning, Optimal Network Reconfiguration, Distributed Generators and Shunt Capacitors integration

1. Introduction

The primary goal of a modern electric power system is to meet consumer demand reliably and cost-effectively. The system comprises three key components: generation, transmission, and distribution. Among these, the Distribution System (DS) plays a critical role in delivering electricity directly to end users. Because DS typically operates at low voltage with high current, it is inherently prone to significant power losses and poor voltage profiles due to structural and operational constraints [1]. Consequently, numerous studies have identified Active Power Loss (APL) reduction as a critical priority in distribution systems. To address this, the most widely adopted strategies include Optimal Network Reconfiguration (ONR), integration of Distributed Generators (DGs), and Shunt Capacitors (SCs), all aimed at minimizing APL while improving Voltage Profile (VP) and system stability [2 – 4]. Notably, growing research attention has shifted toward the combined implementation of ONR with DGs and SCs integration, as this simultaneous approach has proven particularly effective for reducing power losses and enhancing voltage stability.

Optimal network reconfiguration modifies the distribution network topology by toggling switch states between open and closed to achieve a radial configuration that minimizes power losses, improves the voltage profile, and satisfies operational constraints. In recent years, researchers have extensively addressed reconfiguration challenges by developing diverse optimization strategies to reduce losses and enhance voltage profile and stability. To this end, numerous studies have employed advanced meta-heuristic techniques: J. Torres et al. applied a GA based on the edge window decoder (GA-EWD) [5]; Y. Lakshmi Reddy et al. used the Firefly Algorithm (FFA) [6]; E. Azad-Farsani et al. combined Particle Swarm Optimization with TLBO, termed hybrid CPSO-TLBO [7]; S. Teimourzadeh and K. Zare employed Binary Group Search Optimization (BGSO) [8]; R. Sedaghati et al. used an Adaptive Modified Firefly Algorithm (AMFA) [9]; M. Abdelaziz applied a Genetic Algorithm (GA) with varying population sizes [10]; R. Pegado et al. used Binary Particle Swarm Optimization (BPSO) [11]; T. Tran The employed a Chaotic Stochastic Fractal Search Algorithm (CSFSA) [12]; T. T. Nguyen et al. used an Improved Coyote Optimization Algorithm (ICOA) [13]; H. Hizarci et al. applied Time-Varying Acceleration Coefficient Binary PSO (TVAC-BPSO) [14]; and M. Cikan and B. Kekezoglu used an Equilibrium Optimizer (EO) [15] to solve the optimal network reconfiguration problem.

Distributed Generators (DGs) are increasingly integration to modern distribution systems, offering key benefits such as reduced power losses and improved voltage profiles. However, maximizing these benefits without disrupting existing system architecture depends on determining the optimal location and sizing of DGs units, which remains a significant challenge in distribution system planning. To address this issue, researchers have explored numerous advanced meta-heuristic optimization algorithms: U. Sultana et al. applied the Grey Wolf Optimizer (GWO) [16]; D. B. Prakash and C. Lakshminarayana used the Whale Optimization Algorithm (WOA) [17]; S. Kamel employed a Hybrid Gray Wolf Optimizer (HGWO) [18]; J. Radosavljevic et al. used a hybrid phasor PSO and gravitational search algorithm (HPPSOGSA) [19]; G. Deb et al. applied Spider Monkey Optimization (SMO) [20]; A. Selim used improved versions of the Harris Hawks Optimizer (IHHO and MOHHO) [21]; K. H. Truong et al. employed Quasi-Oppositional Chaotic Symbiotic Organisms Search (QOCSOS) [22]; Z. Tan et al. used Swarm Moth Flame Optimization (SMFO) [23]; M. G. Hemeida et al. applied the Manta Ray Foraging Optimization algorithm (MRFO) [24]; and K. S. Sambaiah and T. Jayabarathi used the Salp Swarm Algorithm (SSA) [25] to solve the optimal DG integration problem.

The placement of Shunt Capacitors (SCs) in distribution networks is critical for compensating electrical losses caused by reactive power demand, which can also degrade voltage profiles. It is widely acknowledged that optimally sizing and locating shunt capacitors in Radial Distribution Networks (RDNs) yields significant economic benefits, including reduced peak power and energy losses that offset integration costs while maintaining acceptable voltage levels. To address this challenge, numerous classical mathematical models and modern meta-heuristic optimization approaches have been investigated: Elsheikh et al. applied Particle Swarm Optimization (PSO) [26]; Mohamed Shuaib et al. used the Gravitational Search Algorithm (GSA) [27]; Tamilselvan et al. employed the Flower Pollination Algorithm (FPA) [28]; Dehghani et al. used the Spring Search Algorithm (SSA) [29]; Moghadam et al. applied NSGA-II [30]; Das and Malakar used a Competitive Swarm Optimizer (CSO) [31]; Dixit et al. employed a Gbest-guided Artificial Bee Colony (MGABC) [32]; Jayabarathi et al. used a Hybrid Grey Wolf Optimizer (HGWO) [33]; Mouwafi et al. applied a Chaotic Bat Algorithm (CBA) [34]; and El-Ela et al. used Ant Colony Optimization (ACO) [35] to solve the SC integration problem.

While previous research predominantly focused on optimizing network reconfiguration, DGs, or SCs integration individually, this paper addresses their simultaneous combination to minimize power loss, representing a significant technological advancement. Recent studies have increasingly network reconfiguration with DGs and SCs integration to enhance distribution system efficiency. To resolve this complex optimization problem, researchers have employed various advanced meta-heuristic algorithms: Esmaeili et al. applied a Dedicated Genetic Algorithm (DGA) [36]; Rahiminejad et al. used Modified Teaching-Learning-Based Optimization (MTLBO) [37]; Nguyen et al. employed an Adaptive Cuckoo Search Algorithm (CSA) [38]; Srinivasan and Visalakshi used Autonomous Group Particle Swarm Optimization (AGPSO) [39]; Mohammadi et al. applied Fuzzy-based Bacterial Foraging Optimization

(Fuzzy-BFO) [40]; Salehi et al. used NSGA-II [41]; Tolabi et al. employed the Thief and Police Algorithm (TPA) [42]; Biswal et al. used a Quasi-Reflection-based Slime Mould Algorithm (QRSMA) [43]; Shaheen et al. applied the Artificial Ecosystem Optimizer (AEO) [44]; and Gallego et al. used mixed-integer linear programming (MILP) [45] to solve simultaneous network reconfiguration with DGs and SCs integration.

The FDA [46] is a recently developed nature-inspired metaheuristic that mimics the natural movement of water flow toward the lowest elevation point. Despite its promising performance, the standard FDA suffers from limitations such as premature convergence, insufficient exploration capability, and stagnation in local optima, particularly when applied to complex real-world optimization problems. R. Panda et al. proposed the OFDA [47]; however, the algorithm exhibits slow convergence and has a tendency to become trapped in local optima, which may limit its optimization performance.

To address these shortcomings, researchers have continuously sought improvements through hybridization and modification of existing algorithms. First, a Lévy distribution is used to update the flow velocity vector, enabling a more accurate depiction of the flow's movement toward the neighbour with the smallest objective function value; this introduces a more flexible and random approach to velocity prediction, thereby enhancing the algorithm's capability. Similarly, ROBL is incorporated to refine the decision-making process in flow direction identification, improving the algorithm's adaptability, promoting better exploration of potential solutions, and enhancing overall convergence toward the optimum flow direction. The integration of OBL further strengthens the search mechanism by simultaneously evaluating opposite solutions, accelerating convergence and improving solution diversity. Together, these strategies provide a compelling foundation for overcoming the inherent weaknesses of the standard FDA.

The key contributions of this paper are organized as follows: Section 2 formulates the power loss minimization problem through simultaneous network reconfiguration with DGs and SCs integration. Section 3 presents an overview of the standard FDA along with its proposed modifications. Section 4 reports the simulation results of FDA, OFDA, and MFDA, demonstrating their effectiveness in jointly addressing network reconfiguration with DGs and SCs integration. Section 5 concludes the paper.

2. Problem Formulation

Minimizing power losses is essential to improving the effectiveness of the distribution system. Accordingly, the main contribution of this article is to determine the optimal reconfiguration of the DS together with the integration of DGs and SCs, taking into account the status of switches and tie switches as well as the location and sizing of DGs and SCs units. This article aims to minimize distribution system losses under a given load demand while satisfying operational constraints, as illustrated in the radial-feeder single-line diagram in Fig. 1. The formal mathematical statement of the problem is presented as follows:

$$min\ OF = min(TP_L) \tag{1}$$

where TPL is the total power loss.

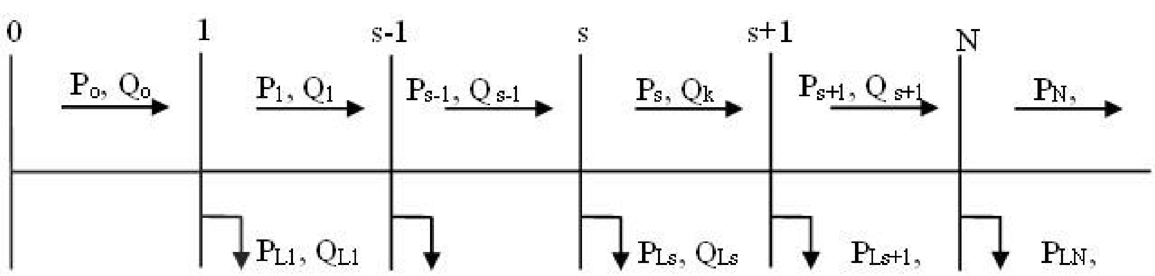

Fig. 1: Radial-feeder Single-line diagram.

Fig. 1 [48] presents the single-line diagram of the radial feeder. The recursive equations below are used to compute the power flow [2, 3, 48], with calculations performed using the backward-forward sweep method via the MATPOWER software tool [49]. The power flow equations are as follows:

$$P_{s+1} = P_s - P_{m,s+1} - R_{s,\ Ls+1} \times \frac{(P_s^2+Q_s^2)}{|V_s|^2}$$
(2)

$$Q_{s+1} = Q_s - Q_{m,s+1} - X_{s,\ Ls+1} \times \frac{(P_s^2+Q_s^2)}{|V_s|^2}$$
(3)

$$|V_{(s+1)}|^2 = |V_s|^2 + 2(R_{s,\ (s+1)} \times P_s + X_{s\ (s+1)} \times Q_s) + (R_{s,\ (s+1)}^2 + X_{s,\ (s+1)}^2)\frac{(P_s^2+Q_s^2)}{|V_s|^2}$$
(4)

"Here P_s and Q_s denote the real and reactive power flowing out of bus s, $P_{L,s+1}$ and $Q_{L,s+1}$ represent real and reactive load powers at bus s+1. The line section connecting buses s and s+1 has resistance R_s, s+1 and reactance X_s, s+1" [49].

The P_{Loss} of the feeder is calculated by

$$P_{Loss}(s,\ s+1) = R_{s,\ Ls+1} \times \frac{(P_s^2+Q_s^2)}{|V_s|^2}$$
(5)

The total P_{Loss} of the feeder is calculated by

$$TP_L = \sum_{s=0}^{n-1} \quad P_{Loss}(s,\ s+1) \tag{6}$$

Here P_{Loss} denotes the total real power loss. This study considers DG units that supply real power, including Type 1 DGs such as Photovoltaic (PV) systems and Wind Turbines (WT). When a DG delivering power output P_{DG} is integrated at bus s, the load at that bus changes from $P_{L,s}$ to ($P_{L,s} - P_{DG}$). Similarly, if bus s has an inductive load of Q_s, integration of a capacitor bank of Q_s units alter the reactive load to ($Q_s - Q_{SC}$). During the search process, the algorithm evaluates all possible equipment locations and ratings to identify the combination that minimizes system losses.

2.1. System Constraints

Bus voltage magnitudes must stay within specified minimum and maximum limits, and branch currents must not exceed rated capacity. These constraints are expressed as follows:

$$V_{min} \leq |V_i| \leq V_{max} \tag{7}$$

$$|I_{s,s+1}| \leq I_{s,s+1(max)} \tag{8}$$

$$P_{DG}^{min} \leq |P_{DG}| \leq P_{DG}^{max} \tag{9}$$

$$Q_{SC}^{min} \leq |Q_{SC}| \leq Q_{SC}^{max} \tag{10}$$

where V_{min} and V_{max} are the minimum and maximum allowable bus voltages, set at 0.90 p.u. and 1.05 p.u., respectively. $I_{s,s+1}$ is the current magnitude in the line between buses s and s+1, and $I_{s,s+1(max)}$ is the maximum permissible current, based on the line's thermal capacity. P_{DG} and Q_{SC} represent the active and reactive power of each DG and SC source, respectively, both constrained within their maximum and minimum limits. For all case studies, the cumulative capacity of DGs and SCs is constrained within the limits specified by [13, 16].

2.2 Performance Indices

The following assessment indices evaluate the effectiveness of the proposed strategy for network reconfiguration combined with optimal DGs and SCs integration. Higher index values indicate a more favourable impact on the distribution system.

APL Reduction Index (APLRI):

APLRI is determined from Eq. (11) [50].

$$APLRI\ (\%) = \frac{TP_{Loss} - TP_{Loss\ (NR+DG+SC)}}{TP_{Loss}} \times 100 \tag{11}$$

TP_{Loss} and $TP_{Loss\ (NR+DG+SC)}$ are the total APL in cases 1 and 5.

RPL Reduction Index (RPLRI):

RPLRI is determined from Eq. (12) [50].

$$RPLRI\ (\%) = \frac{TQ_{Loss} - TQ_{Loss\ (NR+DG+SC)}}{TQ_{Loss}} \times 100 \tag{12}$$

TQ_{Loss} and $TQ_{Loss\ (NR+DG+SC)}$ are the total RPL in cases 1 and 5.

Voltage Profile Improvement (VPI):

VPI is determined from Eq. (13) [50].

$$VPI\ (\%) = \sum_{s=1}^{N_{Bus}} \left(V_{s(0)} - V_{s(NR+DG+SC)}\right)^2 \times 100 \tag{13}$$

where V_s is the sth bus voltage.

3. Flow Direction Algorithms

3.1 Standard Flow Direction Algorithm

Karami et al. [46] developed the Flow Direction Algorithm (FDA) in 2021, based on the D8 technique, which determines the direction of water flow in a drainage basin after transforming rainfall into runoff. Fig. 2 illustrates basin outflow using the D8 method, which generates an initial population within the drainage basin representing the problem's search space. Water flows are then directed toward the lowest elevation point, which corresponds to the best solution.

In the FDA algorithm, the initial position of each flow is calculated as follows:

$$X_{Flow}(i) = lb \times rand \times (ub - lb) \tag{14}$$

where X_{Flow} denotes the water flow position. Additionally, each flow is assumed to have β neighbouring flows, calculated as follows:

$$Neighbour(j) = X_{Flow}(i) + \Delta \times randn \tag{15}$$

Fig. 2: Diagram of basin outflow flow with the D8 technique

Here, neighbour represents the neighbouring flow's position. A small Δ value limits exploration to a narrow range, whereas a large Δ value enables a broader search. To improve the likelihood of approaching the optimal solution, the algorithm performs a wide-ranging global search across diverse regions of the search space, while also conducting a localized search within smaller regions containing promising solutions to refine accuracy. However, excessive global searching can prevent convergence to the required accuracy, while excessive local searching risks entrapment in local optima. To balance these two search strategies, Δ is linearly reduced from its highest to lowest value over the course of the algorithm. To introduce additional diversity, Δ is also directed toward a random location. The mathematical formulation of Δ is given as follows:

$$\Delta = (rand \times X_r - rand \times X_{Flow}(i)) \times \|X_{Best} - X_{Flow}\| \times W \quad (16)$$

Here, X_r denotes a random position, and W is a nonlinear weight assigned a random value between 0 and infinity. The first term describes the movement of $X_{Flow}(i)$ toward a random position (X_r), while the second term reflects that as iterations increase, X_{Flow} converges toward X_{Best}, causing the Euclidean distance between X_{Best} and X_{Flow} to approach zero. W is mathematically formulated as follows:

$$W = \left(\left(1 - \frac{iter}{Max\_iter}\right)^{(2 \times randn)}\right) \times \left(rand \times \frac{iter}{Max\_iter}\right) \times rand \quad (17)$$

Fig. 3 illustrates the variation of W with increasing iterations, which helps prevent the algorithm from becoming trapped in local optima. All water flows move with a velocity (V) toward the neighbour exhibiting the minimum fitness function value.

The velocity of water flow toward neighbouring flows depends on the local slope, mathematically modelled as follows:

$$V = randn \times S_0 \quad (18)$$

Here, S_0 represents the gradient between the current and neighbouring water flows, generating diverse solutions and enhancing global search capability.

Fig. 3: The Changes of W.

The slope of water flow from neighbour i to neighbour j is determined as:

$$S(i,j,d) = \frac{Fitness\_Flow(i) - Neighbor\_Fitness(j)}{\|X_{Flow}(i,d) - Neighbor(j,d)\|} \quad (19)$$

The new position of the water flow is calculated as:

$$X_{FlowNew}(i) = Flow\_X(i) + V \times \frac{X_{Flow}(i) - Neighbor(j)}{|X_{Flow}(i) - Neighbor(j)|} \quad (20)$$

where $X_{FlowNew}(i)$ represents the new position of flow i.

This new flow objective function operates similarly to the sink-filling method for determining flow direction, ensuring that no neighbouring fitness value falls below the current one. The FDA algorithm randomly selects a new flow: if it is less fit than the existing flow, the search continues in that direction; otherwise, it follows the dominant slope direction. Fig. 4 illustrates the position of a sink before and after filling.

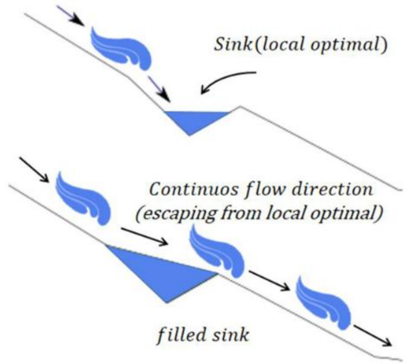

Fig. 4: Position of a sink before and after filling.

Under these conditions, the flow direction is simulated using the following relation:

$$\{if\ FlowFiness(r) < FLowFitness(i)\ FlowNewX(i) = FlowX(i) + randn \times \left(FlowX(r) - FlowX(i)\right)\ else\ FlowNewX(i) = FlowX(i) + 2randn \times \left(BestX - FlowX(i)\right) \tag{21}$$

3.2 Proposed Methodology ROFDA

3.2.1 Lévy Distribution-Based Velocity

A Lévy distribution-based velocity equation can be formulated by incorporating a Lévy flight step into the conventional velocity update, enhancing the algorithm's global exploration capability, as follows:

$$V_{New} = Lévy(dim) \times S_0 \tag{22}$$

The Lévy distribution as follows

$$Lévy = \frac{u}{|v|^{1/\beta}} \tag{23}$$

where $u \sim N(0, \sigma_u^2)$, $v \sim N(0,1)$, $1 < \beta \leq 2$ is the Lévy exponent (typically $\beta = 1.5$).

The standard deviation σ_u is as follows:

$$\sigma_u = \left[\frac{\Gamma(1+\beta)\sin\left(\frac{\pi\beta}{2}\right)}{\Gamma\left(\frac{1+\beta}{2}\right)\beta 2^{(\beta-1)/2}}\right]^{1/\beta} \tag{24}$$

where $\Gamma(\cdot)$ is the Gamma function, β controls the heaviness of the distribution tails.

Table 1: Pseudo Code of ROFDA

Initialize the search agents (X_Flowi) i = 1, . . ., n
Compute the fitness function and create a fitness matrix
Initialize the velocity of flows Vmin and Vmax
while it < itmax
update the W using (Eq. 17)
for all the flows
for all the neighbours

Initialize neighbourhood radius Δj; j = 1, . . ., β using (Eq. 14)

Initialize neighbour flows X_ neighbour

Compute the neighbour fitness function and create a fitness matrix

end (for all the neighbours)

update the slope of a neighbour using (Eq. 19)

if neighbour fitness < flow fitness

update the velocity of each flow using (Eq. 22)

update the new flow using (Eq. 20)

else

update the new flow using (Eq. 21)

end

update the best flow and fitness function

end (for all the flows)

update the new flow OBL with random distribution using (Eq. 26)

end (while)

3.2.2 Random Opposition-Based Learning (ROBL)

Metaheuristic Algorithms (MAs) typically begin with random initial solutions. When these initial solutions lie close to the global solution, the algorithm converges quickly; otherwise, convergence is delayed. To address this challenge and substantially reduce convergence time, Tizhoosh [45] introduced Opposition-Based Learning (OBL) to MAs an efficient strategy that enhances problem-solving performance. OBL is mathematically represented as follows:

$$X_{op} = lb + ub - X \tag{25}$$

where X_{op} denotes the opposite solution, and lb and ub represent the lower and upper bounds, respectively.

As shown in Equation (25), OBL generates the opposite solution at a fixed location, which proves highly effective during the early stages of optimization. However, as optimization progresses, this opposite solution may converge toward a local optimum, causing other individuals to converge toward the same region and resulting in premature convergence and reduced solution accuracy. To address this issue, Wen Long [46] modified OBL by introducing random perturbation into Equation (26), as follows:

$$X_{rop} = lb + ub - rand * X_{rop} \tag{26}$$

where X_{rop} is the new random opposite solution. This Random Opposition-Based Learning (ROBL) approach enhances population diversity and effectively avoids local optima.

4. Results and Discussions

The network reconfiguration with DGs and SCs integration is evaluated on 33-bus and 69-bus test systems to demonstrate the effectiveness and robustness of the proposed ROFDA. Since total system loss depends on the size and location of the integrated DGs and SCs units, adding more units may become technologically or financially impractical. Furthermore, increasing DGs and SCs ratings transforms the network into an active system and raises short-circuit levels. For fair and consistent comparison, this study limits the number of DGs and SCs units to three, in line with prior literature [48], [51]; however, the proposed approach is applicable to any number of units. All test systems are simulated to demonstrate the efficacy and superiority of the proposed method, with the case studies outlined as follows:

Case 1: Base case without network reconfiguration or DGs/SCs integration.

Case 2: Optimal Network Reconfiguration only.

Case 3: DGs Integration only.

Case 4: Fixed SCs Integration only.

Case 5: Optimal Network Reconfiguration with DGs and SCs Integration.

The ROFDA algorithm parameters follow those specified in [46]. The maximum number of iterations is set to 500 for both the 33-bus and 69-bus systems, with a population size of 50 selected based on problem complexity and size. Each test case was simulated 30 times, yielding consistent results with negligible variation across runs. Simulations were performed in MATLAB R2024a on a PC equipped with an 11th -gen Intel Core i5-11300H processor (3.10 GHz) and 8 GB of RAM.

4.1 33 Bus Systems

The test system data follows [48], [49], [52], comprising five tie switches and 32 sectional switches. Fig. 5 shows the system's single-line diagram. The minimum capacity of each DG is restricted to 0.2 MW, and the maximum added capacity is restricted to 2.25 MW. The minimum capacity of each SC is restricted to 0.2 MVAr, and the maximum added capacity is restricted to 2.69 MVAr.

As shown in Table 2, the base case configuration, switches 33, 34, 35, 36, and 37 are open, resulting in active and reactive power losses of 202.66 kW and 135.14 kVAr, respectively, and a minimum voltage of 0.9131 p.u. at bus 18.

Table 2: Comparative Performance Analysis of FDA, OFDA, MFDA, and ROFDA Under Different Optimization Cases for the IEEE 33-Bus.

Case	Details	FDA	OFDA	MFDA	ROFDA
Case 1	TPLoss (kW)	202.66	202.66	202.66	202.66
	TQLoss (kVAr)	135.14	135.14	135.14	135.14
	Vmin (p.u.)	0.9131, 18	0.9131, 18	0.9131, 18	0.9131, 18
Case 2	Open Switches	7, 9, 14, 32, 37	7, 9, 14, 32, 37	7, 9, 14, 32, 37	7, 9, 14, 32, 37
	TPLoss (kW)	139.55	139.55	139.55	139.55
	TQLoss (kVAr)	102.31	102.31	102.31	102.31
	APLRI (%)	31.14	31.14	31.14	31.14
	RPLRI (%)	24.30	24.30	24.30	24.30
	VPI (%)	1.84	1.84	1.84	1.84
	Vmin (p.u.)	0.9378, 32	0.9378, 32	0.9378, 32	0.9378, 32
Case 3	Size in kW (Bus)	733.4, 25	1032.7, 30	1032.7, 30	1032.7, 30
		733.9, 14	733.4, 25	733.9, 14	733.9, 14
		1032.7, 30	733.9, 14	733.4, 25	733.4, 25
	TPLoss (kW)	72.90	72.90	72.90	72.90
	TQLoss (kVAr)	49.91	49.91	49.91	49.91

	APLRI (%)	64.03	64.03	64.03	64.03
	RPLRI (%)	63.07	63.07	63.07	63.07
	VPI (%)	4.59	4.59	4.59	4.59
	Vmin (p.u.)	0.9658, 33	0.9658, 33	0.9658, 33	0.9658, 33
Case 4	Size in kVAr (Bus)	362.5, 13	1007.9, 30	1007.9, 30	1007.9, 30
		1007.9, 30	362.5, 13	362.5, 13	362.5, 13
		1319.6, 3	1319.6, 3	1319.6, 3	1319.6, 3
	TPLoss (kW)	134.01	134.01	134.01	134.01
	TQLoss (kVAr)	89.55	89.55	89.55	89.55
	APLRI (%)	33.88	33.88	33.88	33.88
	RPLRI (%)	33.74	33.74	33.74	33.74
	VPI (%)	1.26	1.26	1.26	1.26
	Vmin (p.u.)	0.9385, 18	0.9385, 18	0.9385, 18	0.9385, 18
Case 5	Open Switches	6, 11, 12, 15, 27	6, 12, 27, 33, 36	7, 14, 15, 26, 35	7, 14, 16, 25, 33
	Size in kW (Bus)	927.2, 29	1221, 30	559.9, 11	996.9, 29
		801.2, 9	511.8, 15	937.8, 25	597.6, 32
		521.6, 18	517.2, 8	752.3, 32	655.5, 9
	Size in kVAr (Bus)	926.3, 3	1119.8, 30	1152.8, 3	1210.6, 30
		559.4, 8	991.8, 3	318.4, 13	451.9, 12
		1204.3, 30	578.4, 9	1218.8, 30	1027.6, 3
	TPLoss (kW)	14.86	15.33	14.12	14.04
	TQLoss (kVAr)	10.89	10.86	10.19	10.16
	APLRI (%)	92.67	92.44	93.03	93.07
	RPLRI (%)	91.94	91.97	92.46	92.48
	VPI (%)	9.59	9.67	9.71	9.77
	Vmin (p.u.)	0.9905, 16	0.9906, 18	0.9908, 16	0.9915, 14

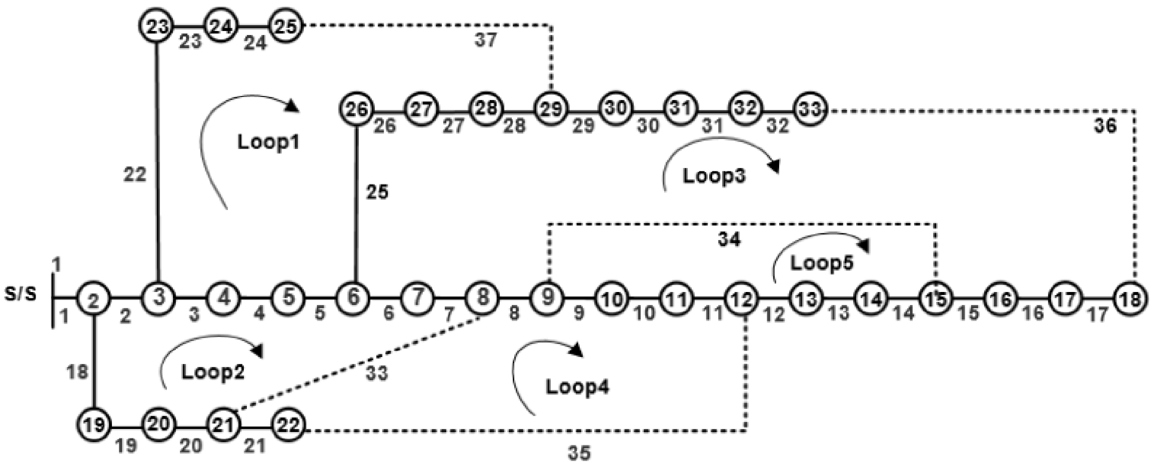

Fig. 5: IEEE-33 bus base configuration.

Case 2 focuses exclusively on network reconfiguration to identify the optimal switch states, with results summarized in Table 2. As shown in Table 2, the ROFDA algorithm identifies the optimal open switches as 7, 9, 14, 32, and 37. Under the given load demand, real and reactive power losses are reduced to 139.55 kW and 102.31 kVAr, respectively, corresponding to active and reactive power loss indices of 31.14% and 24.30%. Table 2 also indicates that the minimum voltage for this load demand is 0.9378 p.u., occurring at bus 32. Additionally, the voltage profile index obtained using ROFDA is 1.84. These results confirm that ROFDA achieves performance comparable to FDA, OFDA, and MFDA when applied solely to optimal network reconfiguration.

In Case 3, the system integrates only the optimal DGs to determine their optimal size and location, with results tabulated in Table 2. As shown in Table 2, the ROFDA algorithm identifies optimal DG locations at buses 30, 14, and 25, with real power injection capacities of 1032.7 kW, 733.9 kW, and 733.4 kW, respectively. Under the given load demand, active and reactive power losses decrease to 72.90 kW and 49.91 kVAr, respectively, corresponding to active and reactive power loss indices of 64.03% and 63.07%. Table 2 also indicates that the minimum voltage for this load demand is 0.9658 p.u., occurring at bus 33. Additionally, the voltage profile index obtained using ROFDA is 4.59. These results confirm that ROFDA achieves performance comparable to FDA, OFDA, and MFDA when applied solely to DGs integration.

In Case 4, the system integrates only the optimal SCs to determine their optimal size and location, with results tabulated in Table 2. As shown in Table 2, the ROFDA algorithm identifies optimal SC locations at buses 30, 13, and 3, with reactive power injection capacities of 1007.9 kVAr, 362.5 kVAr, and 1319.6 kVAr, respectively. Under the given load demand, active and reactive power losses decrease to 134.01 kW and 89.55 kVAr, respectively, corresponding to active and reactive power loss indices of 33.88% and 33.74%. Table 2 also indicates that the minimum voltage for this load demand is 0.9385 p.u., occurring at bus 18. Additionally, the voltage profile index obtained using ROFDA is 1.26. These results confirm that ROFDA achieves performance comparable to FDA, OFDA, and MFDA when applied solely to SCs integration.

In Case 5, network reconfiguration with DGs and SCs integration are performed simultaneously to determine the optimal switch states along with the optimal size and location of DGs and SCs, with results tabulated in Table 2. As shown in Table 2, the ROFDA algorithm identifies the optimal open switches at 7, 14, 16, 25, and 33; optimal DG locations at buses 29, 32, and 9, with real power injection capacities of 996.9 kW, 597.6 kW, and 655.5 kW; and optimal SC locations at buses 30, 12, and 3, with reactive power injection capacities of 1210.6 kVAr, 451.9 kVAr, and 1027.6 kVAr. Under the given load demand, active and reactive power losses decrease to 14.04 kW and 10.16 kVAr, respectively, corresponding to active and reactive power loss indices of 93.07% and 92.48%. Table 2 also indicates that the minimum voltage for this load demand is 0.9915 p.u., occurring at bus 14. Additionally, the voltage profile index obtained using ROFDA is 9.77. These results demonstrate that ROFDA performs effectively for combined network reconfiguration with DGs and SCs integration. The convergence curves for Cases 2 to 5 under the given load demand are shown in Fig. 6(a)–6(d), respectively.

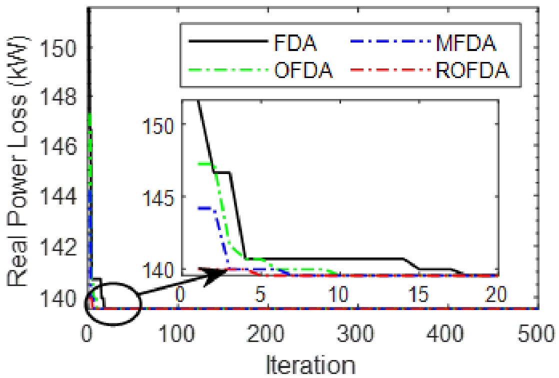

(a) Case 2

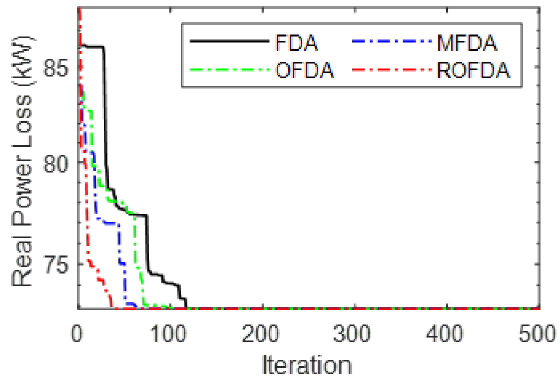

(b) Case 3

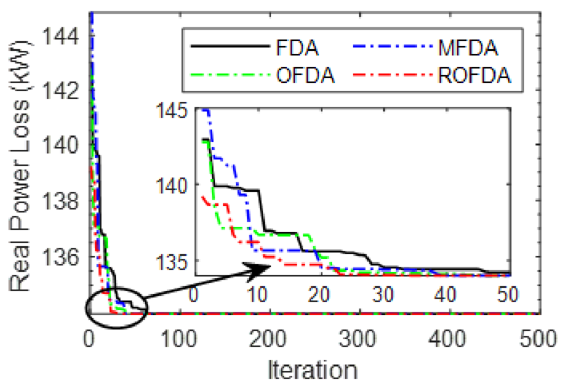

(c) Case 4

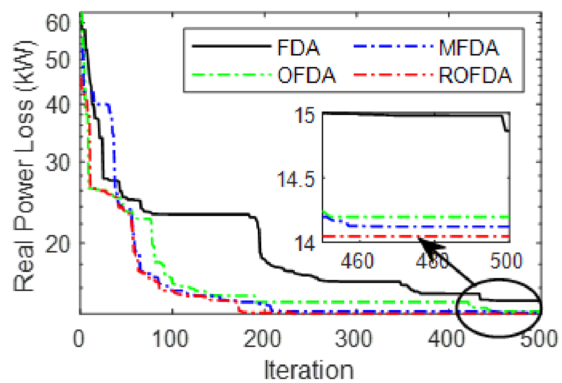

(d) Case 5

Fig. 6: The convergence curve for the given load demand for case 2 and case 5, respectively.

For the given load demand, in Case 2, the APLRI obtained by ROFDA is 31.14%, which is similar to the values achieved by FDA, OFDA, and MFDA. Likewise, the RPLRI obtained by ROFDA is 24.30%, identical to that of FDA, OFDA, and MFDA, while the VPI obtained by ROFDA is 1.84%, again comparable to FDA, OFDA, and MFDA. In Case 3, for the given load demand, the APLRI obtained by ROFDA is 64.03%, identical to the results from FDA, OFDA, and MFDA. The RPLRI obtained by ROFDA is 63.07%, similar to FDA, OFDA, and MFDA, and the VPI obtained by ROFDA is 4.59%, again matching FDA, OFDA, and MFDA. In Case 4, for the given load demand, the APLRI obtained by ROFDA is 33.88%, similar to FDA, OFDA, and MFDA. The RPLRI obtained by ROFDA is 33.74%, identical to FDA, OFDA, and MFDA, and the VPI obtained by ROFDA is 1.26%, again comparable to FDA, OFDA, and MFDA. In Case 5, for the given load demand, the APLRI obtained by ROFDA is 93.07%, a superior outcome compared to FDA, OFDA, and MFDA. The RPLRI obtained by ROFDA is 92.48%, likewise superior to FDA, OFDA, and MFDA, and the VPI improvement achieved by ROFDA is 9.77%, an excellent result compared to FDA, OFDA, and MFDA.

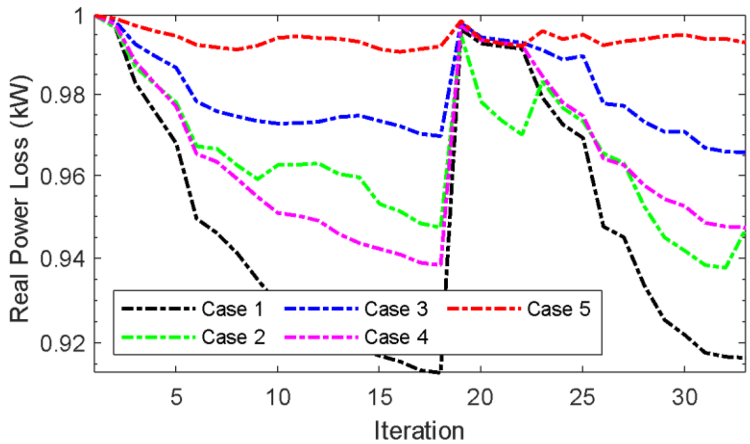

Fig. 7: MFDA obtains the bus voltage of 33-bus for the given load demand in all cases.

In Case 2, FDA, OFDA, MFDA, and ROFDA yield identical results for the given load demand; similarly, in Case 3, their performance remains comparable. In Case 4, FDA, OFDA, MFDA, and ROFDA again produce identical results, whereas in Case 5, ROFDA outperforms FDA, OFDA, and MFDA across all evaluated aspects. Fig. 7 presents the voltage profile for all cases obtained by ROFDA.

4.2 69 Bus Systems

The test system data follows [48], [49], [52], comprising five tie switches and 68 sectional switches, with the single-line diagram shown in Fig. 8. The DG capacity is restricted to a minimum of 0.2 MW and a maximum of 2.5 MW, while the SC capacity is restricted to a minimum of 0.2 MVAr and a maximum of 2.69 MVAr.

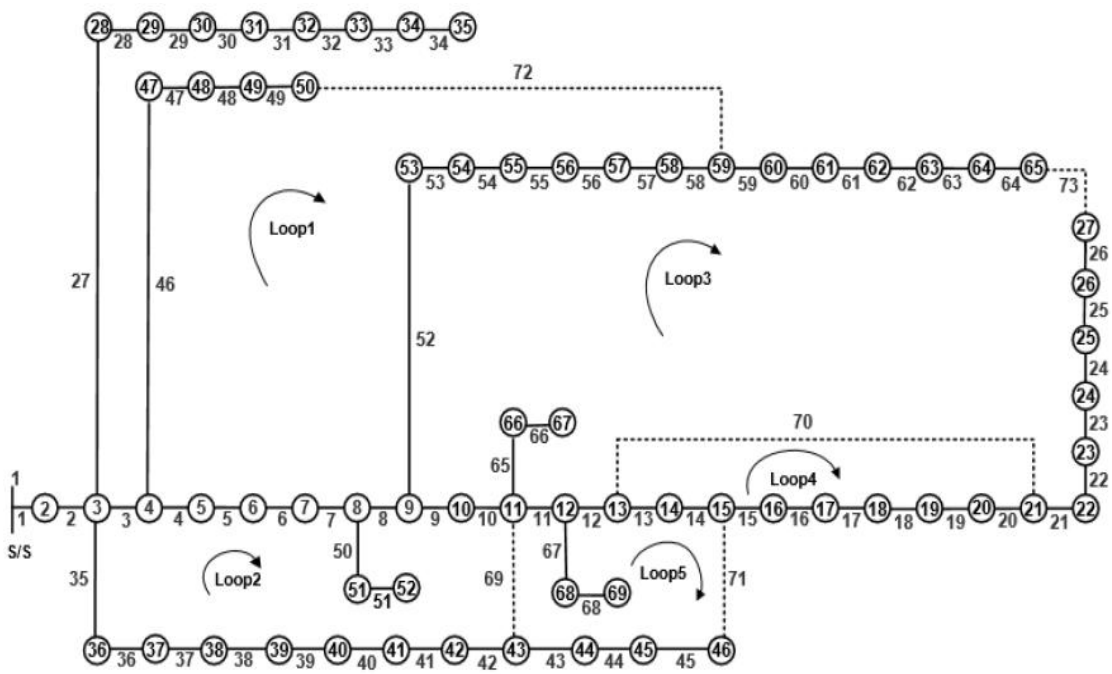

Fig. 8: IEEE-69 bus base configuration

The system network setup begins with the base case, in which switches 69, 70, 71, 72, and 73 are open, resulting in active and reactive power losses of 225 kW and 102.16 kVAr, respectively, and a minimum voltage of 0.9092 p.u. at bus 65.

Case 2 deals exclusively with network reconfiguration to determine the optimal switch states, as presented in Table 3. The results show that ROFDA identifies the optimal open switches as 14, 56, 61, 69, and 70 for the given load demand. Table 3 further shows that active and reactive power losses decrease to 98.61 kW and 92.05 kVAr, respectively, corresponding to active and reactive power loss reduction indices of 56.18% and 9.90%. Additionally, Table 3 indicates that the minimum voltage for the given load demand is 0.9495 p.u. at bus 61, with a voltage profile index of 3.11 obtained from ROFDA. These findings demonstrate that ROFDA performs identically to FDA, OFDA, and MFDA when applied to optimal network reconfiguration alone.

In Case 3, the system integrates only optimal DGs to attain their optimal size and location, with the obtained optimal DG sizes and locations tabulated in Table 3. Table 3 shows that ROFDA identifies the best optimal locations for the given load demand at buses 18, 11, and 61, with real power injection capacities of 380.4, 423.2, and 1696.5 kW, respectively. Table 3 further shows that active and reactive power losses decrease to 69.60 kW and 35.08 kVAr for the load demand, respectively, with active and reactive power loss reduction indices of 69.06% and 65.66% for each loading state. Table 3 also shows that the minimum voltage for the given load demand is 0.9780 p.u. at bus 65. The voltage profile index obtained from ROFDA is 5.67; these findings demonstrate that ROFDA performs identically to FDA, OFDA, and MFDA for DG integration only.

In Case 4, the system integrates only optimal SCs to attain their optimal size and location, with the obtained optimal SC sizes and locations tabulated in Table 3. Table 3 shows that ROFDA identifies the best optimal locations for the given load demand at buses 49, 61, and 12, with reactive power injection capacities of 835.1, 1254.8, and 600.1 kVAr, respectively. Table 3 further shows that active and reactive power losses decrease to 146.03 kW and 66.70 kVAr for the given load demand. Table 3 also shows that active and reactive power loss reduction indices are 35.10% and 34.71% for the load demand, and minimum voltage for the given load demand is 0.9318 p.u. at bus 65. The voltage profile index obtained from ROFDA is 0.62; these findings show that ROFDA works effectively for SC integration only.

In Case 5, network reconfiguration is performed simultaneously with DG and SC integration to determine the optimal switch states along with the optimal size and location of DGs and SCs, with results tabulated in Table 3. The table shows that ROFDA identifies the optimal open switches as 14, 17, 22, 57, and 69, the optimal DG locations at buses 61, 64, and 12 with real power injection capacities of 1370.1, 346, and 533.9 kW, and the optimal SC locations at buses 5, 12, and 61 with reactive power injection capacities of 965, 439.9, and 1285.1 kVAr. Table 3 further shows that active and reactive power losses decrease to 5.21 kW and 7.38 kVAr for the given load demand, corresponding to active and reactive power loss reduction indices of 97.68% and 92.78%, respectively. The minimum voltage for the given load demand is 0.9933 p.u. at bus 23, with a voltage profile index of 8.51 obtained from ROFDA. These findings confirm that ROFDA performs effectively for combined network reconfiguration with DGs and SCs integration. The convergence curves for the given load demand under Cases 2, 3, 4, and 5 are shown in Fig. 9(a)–9(d), respectively.

Table 3: Comparative Performance Analysis of FDA, OFDA, MFDA, and ROFDA Under Different Optimization Cases for the IEEE 69-Bus.

Case	**Details**	**FDA**	**OFDA**	**MFDA**	**ROFDA**
Case 1	TPLoss (kW)	225.00	225.00	225.00	225.00
	TQLoss (kVAr)	102.16	102.16	102.16	102.16
	Vmin (p.u.)	0.9092, 65	0.9092, 65	0.9092, 65	0.9092, 65
Case 2	Open Switches	14, 56, 61, 69, 70	14, 56, 61, 69, 70	14, 56, 61, 69, 70	14, 56, 61, 69, 70
	TPLoss (kW)	98.61	98.61	98.61	98.61
	TQLoss (kVAr)	92.05	92.05	92.05	92.05
	APLRI (%)	56.18	56.18	56.18	56.18
	RPLRI (%)	9.90	9.90	9.90	9.90

	VPI (%)	3.11	3.11	3.11	3.11
	V_{min} (p.u.)	0.9495, 61	0.9495, 61	0.9495, 61	0.9495, 61
Case 3	Size in kW (Bus)	1709.2, 61	1709.2, 61	380.4, 18	380.4, 18
		394.2, 66	396.6, 18	423.2, 11	423.2, 11
		396.6, 18	394.2, 66	1696.5, 61	1696.5, 61
	TP_{Loss} (kW)	69.78	69.78	69.60	69.60
	TQ_{Loss} (kVAr)	35.13	35.13	35.08	35.08
	APLRI (%)	68.99	68.99	69.06	69.06
	RPLRI (%)	65.61	65.61	65.66	65.66
	VPI (%)	5.60	5.67	5.67	5.67
	V_{min} (p.u.)	0.9776, 65	0.978, 65	0.978, 65	0.978, 65
Case 4	Size in kVAr (Bus)	359, 17	1058.3, 5	381.6, 17	835.1, 49
		1058.3, 5	359, 17	1298, 61	1254.8, 61
		1272.7, 61	1272.7, 61	1010.5, 49	600.1, 12
	TP_{Loss} (kW)	146.42	146.42	146.16	146.03
	TQ_{Loss} (kVAr)	68.25	68.25	67.45	66.70
	APLRI (%)	34.93	34.93	35.04	35.10
	RPLRI (%)	33.20	33.20	33.97	34.71
	VPI (%)	0.59	0.59	0.61	0.62
	V_{min} (p.u.)	0.9313, 65	0.9313, 65	0.9316, 65	0.9318, 65
Case 5	Open Switches	13, 19, 22, 55, 69	14, 17, 55, 64, 69	13, 16, 55, 69, 73	14, 17, 22, 57, 69
	Size in kW (Bus)	1612.5, 61	439.2, 21	302.3, 21	1370.1, 61
		371.2, 12	200, 66	310.1, 12	346, 64
		266.2, 50	1610.8, 61	1637.6, 61	533.9, 12
	Size in kVAr (Bus)	1214.2, 61	522, 12	1245.1, 61	965, 5
		491.9, 66	1203.1, 61	509.3, 12	439.9, 12
		983.9, 49	964.9, 5	935.5, 5	1285.1, 61
	TP_{Loss} (kW)	6.11	5.41	5.31	5.21
	TQ_{Loss} (kVAr)	6.40	7.39	7.45	7.38
	APLRI (%)	97.28	97.59	97.64	97.68
	RPLRI (%)	93.74	92.77	92.71	92.78
	VPI (%)	8.51	8.68	8.78	8.52
	V_{min} (p.u.)	0.9938, 18	0.9942, 64	0.9925, 65	0.9933, 23

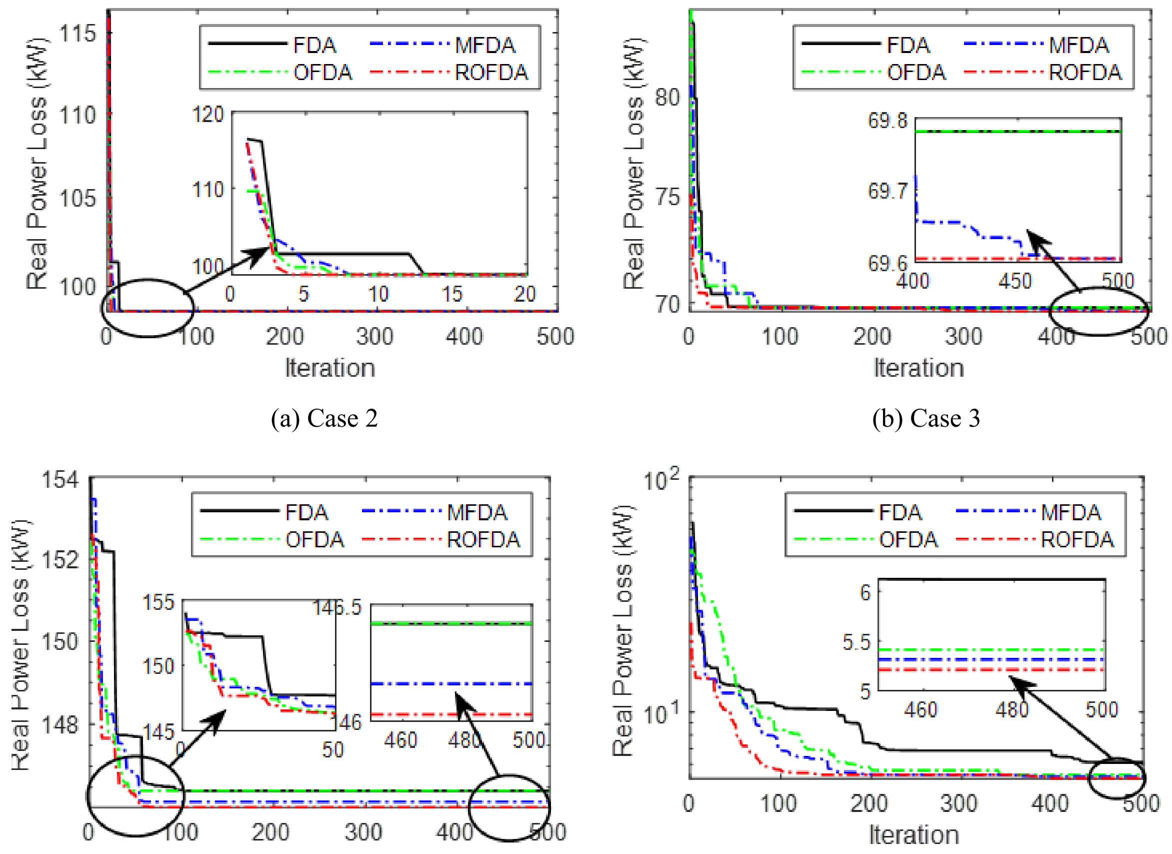

(a) Case 2 (b) Case 3

I Case 4 (d) Case 5

Fig. 9: The convergence curve for the given load demand for case 2 to case 5, respectively.

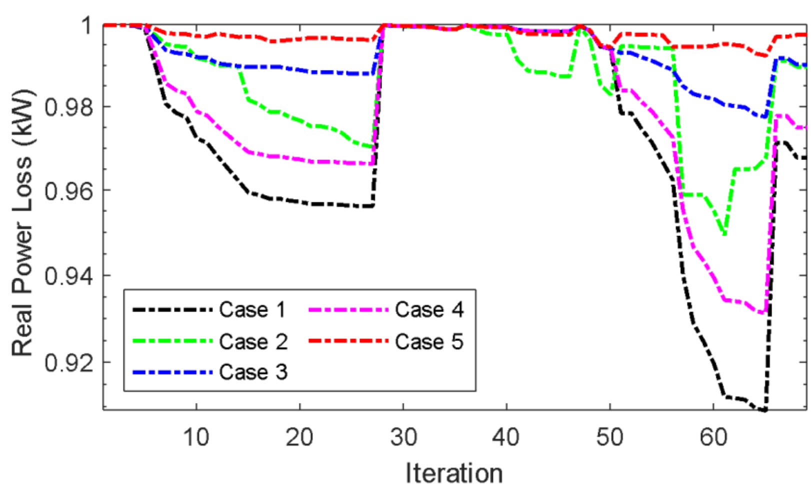

Fig. 10: ROFDA obtains the bus voltage of 69-bus for the given load demand in all cases.

In Case 2, for the given load demand, the APLRI obtained by ROFDA is 56.18%, which is similar to FDA, OFDA, and MFDA, and the value of RPLRI obtained from ROFDA is 9.90%, which is identical to FDA, OFDA, and MFDA; the VPI improvement obtained from ROFDA is 3.11%, which is similar to FDA, OFDA, and MFDA. In Case 3, for the given load demand, the APLRI obtained by ROFDA is 69.06%, which is a superior outcome compared to

FDA and OFDA, and identical to MFDA, and the value of RPLRI obtained from ROFDA is 65.66%, which is a superior outcome compared to FDA and OFDA, and identical to MFDA; the VPI obtained from ROFDA is 5.67%, which is a superior outcome compared to FDA, and identical to OFDA and MFDA. In Case 4, for the given load demand, the APLRI obtained by ROFDA is 35.04%, which is a superior outcome compared to FDA and OFDA, and identical to MFDA, and the value of RPLRI obtained from ROFDA is 33.97%, which is a superior outcome compared to FDA and OFDA, and identical to MFDA; the VPI obtained from ROFDA is 0.61%, which is a superior outcome compared to FDA and OFDA, and identical to MFDA. In Case 5, for the given load demand, the APLRI obtained by ROFDA is 97.68%, which is a superior outcome compared to FDA, OFDA, and MFDA, and the value of RPLRI obtained from ROFDA is 92.78%, which is a superior outcome compared to FDA, OFDA, and MFDA; the VPI obtained from ROFDA is 8.80%, which is a superior outcome compared to FDA, OFDA, and MFDA.

For the given load demand, in Case 2, FDA, OFDA, MFDA, and ROFDA yield identical results across the three loading conditions. In Case 3, ROFDA produces superior outcomes compared to FDA and OFDA, while performing identically to MFDA. In Case 4, ROFDA again outperforms FDA and OFDA, with results matching MFDA. In Case 5, ROFDA delivers superior outcomes across all metrics compared to FDA, OFDA, and MFDA across all evaluated aspects. Fig. 10 presents the voltage profile for all cases obtained by ROFDA.

5. Conclusions

This article presents an efficient implementation of ROFDA for simultaneous ONR with DGs and SCs integration. Power losses were evaluated across four approaches: ONR alone, DGs integration alone, SCs integration alone, and simultaneous ONR with DGs and SCs integration. Among these, the simultaneous approach proved most effective at reducing power losses and improving the voltage profile. For the given load demand, ROFDA achieved the lowest power losses under simultaneous ONR with DGs and SCs integration, reducing losses by 93.07% for the 33-bus system and 5.21% for the 69-bus system, while improving the minimum voltage to 0.9915 p.u. and 0.9933 p.u., respectively. These results confirm that ROFDA is a reliable and efficient technique for simultaneous ONR with DGs and SCs integration across both test systems, consistently yielding better voltage profiles and lower power losses than FDA, OFDA, and MFDA. Overall, ROFDA offers an effective solution for ONR, DGs and SCs integration individually, or their simultaneous implementation.

REFERENCES

1. Nguyen, T. T., Truong, A. V., & Phung, T. A. (2016). A novel method based on adaptive cuckoo search for optimal network reconfiguration and distributed generation allocation in distribution network. International Journal of Electrical Power & Energy Systems, 78, 801–815.
2. Rahiminejad, A., Hosseinian, S. H., Vahidi, B., & Shahrooyan, S. (2016). Simultaneous Distributed Generation Placement, Capacitor Placement, and Reconfiguration using a Modified Teaching-Learning-based Optimization Algorithm. Electric Power Components and Systems, 44(14), 1631–1644.
3. Salehi, J., Oskuee, M. R. J., & Amini, A. (2018). Stochastics multi-objective modelling of simultaneous reconfiguration of power distribution network and allocation of DGs and capacitors. *International Journal of Ambient Energy*, *39*(2), 176–187.
4. Tolabi, H. B., Ara, A. L., & Hosseini, R. (2020). A new thief and police algorithm and its application in simultaneous reconfiguration with optimal allocation of capacitor and distributed generation units. Energy, 203, 117911.
5. J. Torres, J. L. Guardado, F. Rivas-Dávalos, S. Maximov, and E. Melgoza, “A genetic algorithm based on the edge window decoder technique to optimize power distribution systems reconfiguration,” *International Journal of Electrical Power and Energy Systems*, vol. 45, no. 1, pp. 28–34, Feb. 2013.
6. Y. Lakshmi Reddy, T. Sathiyanarayanan, and M. Sydulu, “Application of firefly algorithm for radial distribution network reconfiguration using different loads,” in *IFAC Proceedings Volumes (IFAC-PapersOnline)*, 2014, vol. 3, no. PART 1, pp. 700–705.
7. E. Azad-Farsani, M. Zare, R. Azizipanah-Abarghooee, and H. Askarian-Abyaneh, “A new hybrid CPSO-TLBO optimization algorithm for distribution network reconfiguration,” *Journal of Intelligent and Fuzzy Systems*, vol. 26, no. 5, pp. 2175–2184, 2014.
8. S. Teimourzadeh and K. Zare, “Application of binary group search optimization to distribution network reconfiguration,” *International Journal of Electrical Power and Energy Systems*, vol. 62, pp. 461–468, 2014.
9. R. Sedaghati, M. Hakimzadeh, H. Fotoohabadi, and A. R. Rajabi, “Study of network reconfiguration in distribution systems using an Adaptive Modified Firefly Algorithm,” *Automatika*, vol. 57, no. 1, pp. 27–36, 2016.

10. M. Abdelaziz, “Distribution network reconfiguration using a genetic algorithm with varying population size,” *Electric Power Systems Research*, vol. 142, pp. 9–11, Jan. 2017.
11. R. Pegado, Z. Ñaupari, Y. Molina, and C. Castillo, “Radial distribution network reconfiguration for power losses reduction based on improved selective BPSO,” *Electric Power Systems Research*, vol. 169. Elsevier Ltd, pp. 206–213, Apr. 01, 2019.
12. T. Tran The, D. Vo Ngoc, and N. Tran Anh, “Distribution Network Reconfiguration for Power Loss Reduction and Voltage Profile Improvement Using Chaotic Stochastic Fractal Search Algorithm,” *Complexity*, vol. 2020, 2020.
13. T. T. Nguyen, Q. T. Nguyen, and T. T. Nguyen, “Optimal radial topology of electric unbalanced and balanced distribution system using improved coyote optimization algorithm for power loss reduction,” *Neural Comput Appl*, vol. 33, no. 18, pp. 12209–12236, Sep. 2021.
14. H. Hizarci, O. Demirel, and B. E. Turkay, “Distribution network reconfiguration using time-varying acceleration coefficient assisted binary particle swarm optimization,” *Engineering Science and Technology, an International Journal*, vol. 35, Nov. 2022.
15. M. Cikan and B. Kekezoglu, “Comparison of metaheuristic optimization techniques including Equilibrium optimizer algorithm in power distribution network reconfiguration,” *Alexandria Engineering Journal*, vol. 61, no. 2, pp. 991–1031, Feb. 2022.
16. U. Sultana, A. B. Khairuddin, A. S. Mokhtar, N. Zareen, and B. Sultana, “Grey wolf optimizer-based placement and sizing of multiple distributed generation in the distribution system,” Energy, vol. 111, pp. 525–536, Sep. 2016.
17. D. B. Prakash and C. Lakshminarayana, “Multiple DG placements in radial distribution system for multi objectives using Whale Optimization Algorithm,” Alexandria Engineering Journal, vol. 57, no. 4, pp. 2797–2806. Dec. 2018.
18. S. Kamel, A. Awad, H. Abdel-Mawgoud, and F. Jurado, “Optimal DG allocation for enhancing voltage stability and minimizing power loss using hybrid gray Wolf optimizer,” *Turkish Journal of Electrical Engineering and Computer Sciences*, vol. 27, no. 4, pp. 2947–2961, 2019.
19. J. Radosavljevic, N. Arsic, M. Milovanovic, and A. Ktena, “Optimal Placement and Sizing of Renewable Distributed Generation Using Hybrid Metaheuristic Algorithm,” Journal of Modern Power Systems and Clean Energy, vol. 8, no. 3, pp. 499–510, May 2020.
20. G. Deb, K. Chakraborty, and S. Deb, “Modified Spider Monkey Optimization-Based Optimal Placement of Distributed Generators in Radial Distribution System for Voltage Security Improvement,” Electric Power Components and Systems, vol. 48, no. 9–10, pp. 1006–1020, Oct. 2020.
21. Selim, S. Kamel, A. S. Alghamdi, and F. Jurado, “Optimal Placement of DGs in Distribution System Using an Improved Harris Hawks Optimizer Based on Single- And Multi-Objective Approaches,” *IEEE Access*, vol. 8, pp. 52815–52829, 2020.
22. K. H. Truong, P. Nallagownden, I. Elamvazuthi, and D. N. Vo, “A Quasi-Oppositional-Chaotic Symbiotic Organisms Search algorithm for optimal allocation of DG in radial distribution networks,” *Applied Soft Computing Journal*, vol. 88, Mar. 2020.
23. Z. Tan, M. Zeng, and L. Sun, “Optimal Placement and Sizing of Distributed Generators Based on Swarm Moth Flame Optimization,” *Front Energy Res*, vol. 9, Apr. 2021.
24. M. G. Hemeida, A. A. Ibrahim, A. A. A. Mohamed, S. Alkhalaf, and A. M. B. El-Dine, “Optimal allocation of distributed generators DG based Manta Ray Foraging Optimization algorithm (MRFO),” *Ain Shams Engineering Journal*, vol. 12, no. 1, pp. 609–619, Mar. 2021.
25. K. S. Sambaiah and T. Jayabarathi, “Optimal reconfiguration and renewable distributed generation allocation in electric distribution systems,” *International Journal of Ambient Energy*, vol. 42, no. 9, pp. 1018–1031, 2021.
26. Elsheikh, A., Helmy, Y., Abouelseoud, Y., & Elsherif, A. (2014). Optimal capacitor placement and sizing in radial electric power systems. Alexandria Engineering Journal, 53(4), 809–816.
27. Mohamed Shuaib, Y., Surya Kalavathi, M., & Christober Asir Rajan, C. (2015). Optimal capacitor placement in radial distribution system using Gravitational Search Algorithm. International Journal of Electrical Power & Energy Systems, 64, 384–397.
28. Tamilselvan, V., Jayabarathi, T., Raghunathan, T., & Yang, X. S. (2018). Optimal capacitor placement in radial distribution systems using flower pollination algorithm. Alexandria Engineering Journal, 57(4), 2775–2786.
29. Dehghani, M., Montazeri, Z., & Malik, O. P. (2020). Optimal Sizing and Placement of Capacitor Banks and Distributed Generation in Distribution Systems Using Spring Search Algorithm. International Journal of Emerging Electric Power Systems, 21(1).
30. Moghadam, M. E., Falaghi, H., & Farhadi, M. (2020). A Novel Method of Optimal Capacitor Placement in the Presence of Harmonics for Power Distribution Network Using NSGA-II Multi-Objective Genetic Optimization Algorithm. Mathematical and Computational Applications 2020, Vol. 25, Page 17, 25(1), 17.
31. Das, S., & Malakar, T. (2021). Optimal capacitor placement and sizing in a distribution system using a competitive swarm optimizer algorithm. International Journal of Advanced Intelligence Paradigms, 20(1–2), 89–125.
32. Dixit, M., Kundu, P., & Jariwala, H. R. (2018). Optimal integration of shunt capacitor banks in distribution networks for assessment of techno-economic asset. Computers & Electrical Engineering, 71, 331–345.
33. Jayabarathi, T., Raghunathan, T., Sanjay, R., Jha, A., Mirjalili, S., & Cherukuri, S. H. C. (2022). Hybrid Grey Wolf Optimizer Based Optimal Capacitor Placement in Radial Distribution Systems. Electric Power Components and Systems, 50(8), 413–425.

34. Mouwafi, M. T., El-Sehiemy, R. A., & El-Ela, A. A. A. (2022). A two-stage method for optimal placement of distributed generation units and capacitors in distribution systems. Applied Energy, 307, 118188.
35. El-Ela, A. A. A., Mouwafi, M. T., & Elbaset, A. A. (2023). Optimal Capacitor Placement for Power Loss Reduction and Voltage Profile Improvement. Modern Optimization Techniques for Smart Grids, 107–139.
36. Esmaeili, D., Zare, K., Mohammadi-Ivatloo, B., & Nojavan, S. (2015). Simultaneous Optimal Network Reconfiguration, DG and Fixed/Switched Capacitor Banks Placement in Distribution Systems using Dedicated Genetic Algorithm. In Majlesi Journal of Electrical Engineering (Vol. 9, Issue 4).
37. Rahiminejad, A., Hosseinian, S. H., Vahidi, B., & Shahrooyan, S. (2016). Simultaneous Distributed Generation Placement, Capacitor Placement, and Reconfiguration using a Modified Teaching-Learning-based Optimization Algorithm. Electric Power Components and Systems, 44(14), 1631–1644.
38. Nguyen, T. T., Truong, A. V., & Phung, T. A. (2016). A novel method based on adaptive cuckoo search for optimal network reconfiguration and distributed generation allocation in distribution network. International Journal of Electrical Power & Energy Systems, 78, 801–815.
39. Srinivasan, G., & Visalakshi, S. (2017). Application of AGPSO for Power loss minimization in Radial Distribution Network via DG units, Capacitors and NR. Energy Procedia, 117, 190–200.
40. Mohammadi, M., Rozbahani, A. M., & Bahmanyar, S. (2017). Power loss reduction of distribution systems using BFO based optimal reconfiguration along with DG and shunt capacitor placement simultaneously in fuzzy framework. Journal of Central South University, 24(1), 90–103.
41. Salehi, J., Oskuee, M. R. J., & Amini, A. (2018). Stochastics multi-objective modelling of simultaneous reconfiguration of power distribution network and allocation of DGs and capacitors. International Journal of Ambient Energy, 39(2), 176–187.
42. Tolabi, H. B., Ara, A. L., & Hosseini, R. (2020). A new thief and police algorithm and its application in simultaneous reconfiguration with optimal allocation of capacitor and distributed generation units. Energy, 203, 117911.
43. Biswal, S. R., Shankar, G., Elavarasan, R. M., & Mihet-Popa, L. (2021). Optimal Allocation/Sizing of DGs/Capacitors in Reconfigured Radial Distribution System Using Quasi-Reflected Slime Mould Algorithm. IEEE Access, 9, 125658–125677.
44. Shaheen, A., Elsayed, A., Ginidi, A., El-Sehiemy, R., & Elattar, E. (2022). Reconfiguration of electrical distribution network-based DG and capacitors allocations using artificial ecosystem optimizer: Practical case study. Alexandria Engineering Journal, 61(8), 6105–6118.
45. Gallego, L. A., Lopez-Lezama, J. M., & Carmona, O. G. (2022). A Mixed-Integer Linear Programming Model for Simultaneous Optimal Reconfiguration and Optimal Placement of Capacitor Banks in Distribution Networks. IEEE Access, 10, 52655–52673.
46. H. Karami, M. V. Anaraki, S. Farzin, and S. Mirjalili, "Flow Direction Algorithm (FDA): A Novel Optimization Approach for Solving Optimization Problems," *Comput Ind Eng*, vol. 156, Jun. 2021,
47. R. Panda, M. Swain, M. K. Naik, S. Agrawal, and A. Abraham, "A Novel Practical Decisive Row-class Entropy-based Technique for Multilevel Threshold Selection Using Opposition Flow Directional Algorithm," IEEE Access, p. 1, 2022.
48. P. P. Biswas, R. Mallipeddi, P. N. Suganthan, and G. A. J. Amaratunga, "A multiobjective approach for optimal placement and sizing of distributed generators and capacitors in distribution network," Appl. Soft Comput. J., vol. 60, pp. 268–280, 2017.
49. R. D. Zimmerman, C. E. Murillo-Sánchez, and R. J. Thomas, "MATPOWER: Steady-state operations, planning, and analysis tools for power systems research and education," IEEE Trans. Power Syst., vol. 26, no. 1, pp. 12–19, Feb. 2011.
50. H. Teimourzadeh and B. Mohammadi-Ivatloo, "A three-dimensional group search optimization approach for simultaneous planning of distributed generation units and distribution network reconfiguration," Appl Soft Comput, vol. 88, Mar. 2020.
51. S. Sambaiah and T. Jayabarathi, "Optimal reconfiguration and renewable distributed generation allocation in electric distribution systems," International Journal of Ambient Energy, vol. 42, no. 9, pp. 1018–1031, 2021.
52. R. S. Rao, K. Ravindra, K. Satish, and S. V. L. Narasimham, "Power loss minimization in distribution system using network reconfiguration in the presence of distributed generation," IEEE Transactions on Power Systems, vol. 28, no. 1, pp. 317–325, 2013.